INDERSCIENCE PUBLISHERS
Linking academia, business and industry through research

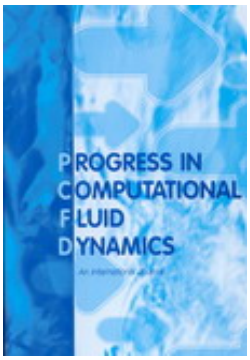

Progress in Computational Fluid Dynamics, An International Journal

ISSN online: 1741-5233 - ISSN print: 1468-4349
https://www.inderscience.com/pcfd

Quantifying wall effects on spherical particle settling with the Lattice Boltzmann method

Abhijeet D. Chodankar, Michael Poirier, John Dekarske, Will Baggett, Davide Dapelo, Dwayne McDaniel, Michael C. Sukop

DOI: 10.1504/PCFD.2026.10079012

Article History:

Received:	30 July 2025
Last revised:	22 April 2026
Accepted:	23 April 2026
Published online:	16 June 2026

Quantifying wall effects on spherical particle settling with the Lattice Boltzmann method

Abhijeet D. Chodankar

Department of Mechanical and Materials Engineering,
Florida International University,
Miami, 33174, Florida, USA
Email: achod002@fiu.edu

Michael Poirier, John Dekarske and Will Baggett

Savannah River National Laboratory,
Savannah River Site,
Aiken, SC 29808, South Carolina, USA
Email: mrp1980a@gmail.com
Email: john.dekarske@srnl.doe.gov
Email: will.baggett@srnl.doe.gov

Davide Dapelo

Department of Civil and Environmental Engineering,
School of Engineering,
University of Liverpool,
The Quadrangle, Brownlow Hill,
Liverpool L69 3GH, UK
Email: d.dapelo@liverpool.ac.uk

Dwayne McDaniel

Department of Mechanical and Materials Engineering,
Florida International University,
Miami, 33174, Florida, USA
Email: mcdaniel@fiu.edu

Michael C. Sukop*

Department of Earth and Environment,
Institute of Environment,
Florida International University,
Miami, 33199, Florida, USA
Email: sukopm@fiu.edu
*Corresponding author

Abstract: Understanding sedimentation relies on grasping the physics between a particle and a fluid. This research employs the Lattice Boltzmann method to conduct a benchmarking study on the sedimentation of a single spherical particle in a Newtonian fluid. The study explores the effects of particle diameter, particle density, and walls on particle settling behaviour. The methods employed include the point particle method and the homogeneous Lattice Boltzmann method (HLBM) using the OpenLB code. The primary objectives of this research are to calculate terminal settling velocity, analyse velocity and vorticity profiles, and track particle trajectories. The HLBM excels in providing precise flow representation around particles, whereas the point particle method shows limitations at higher particle Reynolds numbers. Additionally, the research reveals that wall effects reduce terminal settling velocity and shorten wake length. The domain-size-to-particle-size ratios at which wall-induced vortices disappear for various particle properties are identified. Thorough understanding of the settling physics of a single particle should contribute to unravelling the settling dynamics of multiple particles.

Keywords: homogeneous Lattice Boltzmann method; HLBM; two-way coupling; particle diameter; particle density; wall effects.

Reference to this paper should be made as follows: Chodankar, A.D., Poirier, M., Dekarske, J., Baggett, W., Dapelo, D., McDaniel, D. and Sukop, M.C. (2026) 'Quantifying wall effects on spherical particle settling with the Lattice Boltzmann method', *Progress in Computational Fluid Dynamics*, Vol. 26, No. 7, pp.1–12.

Biographical notes: Abhijeet D. Chodankar is a Postdoctoral Appointee at Argonne National Laboratory, where he works in the field of batteries. He earned a BE in Mechanical Engineering from Goa University, India, where his undergraduate research focused on improving cooling tower efficiency. He later received an MS in Petroleum Engineering from the University of Louisiana at Lafayette, where he developed a coupled fluid axial-lateral drill string vibration model based on classical vibration theory. He completed his PhD in Mechanical Engineering at Florida International University, applying the Lattice Boltzmann Method in computational fluid dynamics to study particle dynamics such as sedimentation, plugging, and resuspension in ion-exchange columns. His research interests encompass batteries, computational fluid dynamics, solid mechanics, mechanical vibrations, fluid-structure interaction, and optimisation.

Michael Poirier is a Senior Fellow Engineer at the Savannah River National Laboratory (retired). He has over 30 years of experience developing processes to treat radioactive waste at the Savannah River Site and Hanford. His areas of focus are fluid mixing, non-Newtonian fluids, and solid-liquid separation. His work has included laboratory experimentation, pilot-scale experimentation, and computer modelling. He obtained a BS in Chemical Engineering from the University of Notre Dame, and a PhD in Chemical Engineering from the University of Illinois at Urbana-Champaign.

John Dekarske is a Scientist at Savannah River National Laboratory. He has a MA in Chemistry from the University of Virginia. His current research is on characterising high level waste in the tank farms at the Savannah River Site for salt batches, sludge batches, and pre-closure samples.

Will Baggett is an R&D Engineer at Savannah River National Laboratory's Engineering Development Lab. Holding a BSc in Mechanical Engineering from New Mexico State University, his work centers on large-scale experimentation, process development for waste immobilisation, system mixing, and waste treatment technologies.

Davide Dapelo graduated in Theoretical Physics from the University of Genoa, Italy, in 2010 and obtained a PhD in Civil Engineering from the University of Birmingham, UK, in 2016. He subsequently held postdoctoral research positions at the Universities of Birmingham and Bradford. In January 2022, he was appointed Lecturer in Civil Engineering at the University of Bradford before joining the University of Liverpool as Lecturer in Civil Engineering in September 2022.

Dwayne McDaniel is currently an Associate Professor in Florida International University's Department of Mechanical and Materials Engineering. He received his BS in Aerospace Engineering from the University of Florida and his MS and PhD in Engineering Mechanics, also from the University of Florida. He has approximately twenty-five years of experience related to research and analysis in mechanical and aerospace engineering and is a registered professional engineer in the State of Florida. His research interests include experimental and computational fluid mechanics and sensors and robotics. At FIU, his responsibilities have included directing and executing research related to mechanical and aerospace applications for the federal government and the private sector.

Michael C. Sukop is Professor of Hydrogeology at Florida International University. He earned his BS in 1982 in Geosciences at The Pennsylvania State University, and his MS in 1989 and PhD in 2001 in Soil Physics at Washington State University and the University of Kentucky, respectively. He co-authored two books on Lattice Boltzmann modelling.

1 Introduction

Fluids often contain particles of various shapes, densities, and sizes. Particles can exist as a single particle or as aggregates of particles. The settling time of particles can be estimated using their established terminal settling velocities with recognition of the different conditions that affect settling velocity. Particle-fluid, particle-particle, and particle-wall interactions play critical roles in particle settling and ultimate sedimentation.

The terminal settling velocity of a particle at low Reynolds number ($Re = \frac{ud}{\nu}$, where u the settling velocity, d is the particle diameter, and ν is the kinematic viscosity of the fluid), can be estimated using Stokes law as: $u = \frac{1}{18}\frac{(\rho_s/\rho - 1)gd^2}{\nu}$, where ρ_s is the particle density, ρ is the fluid density, and g is the magnitude of gravitational acceleration. The terminal settling velocity increases with an increase in particle diameter and particle density and decreases with an increase in liquid density and liquid viscosity. The limitations of Stokes law include the assumption of a spherical particle shape, smooth surfaces, a fluid flow regime with Reynolds number less than 1, homogeneous particle material, no inertial effects, and no particle-particle interactions. Additionally, the terminal

settling velocity should be measured in an infinite domain if it is to match the Stokes law prediction. Wray (1977) revisits Stokes law and its limitations.

In practice, spherical particles can be rougher, denser, and larger than those that meet the smoothness and low Re requirements in a particular fluid. Nielsen (1993) attributed the reduction of the settling velocities at higher Re to nonlinear drag and related vortex trapping and particle loitering phenomena, sometimes attributable to larger, denser, and/or rougher particles. Jenny et al. (2004) and Veldhuis and Biesheuvel (2007) employed the Galileo number to categorise the behaviour of particle trajectories. The Galileo number G is defined as follows: $G = \frac{\sqrt{(\rho_s/\rho - 1)gd^3}}{\nu}$. The Galileo number includes relevant variables for any case of a single particle under gravity in infinite fluid. Together with the particle/fluid density ratio ρ_s/ρ, the settling behaviour of particles can be predicted (Jenny et al., 2004). Settling is expected to be axisymmetric (i.e., no unsteady wakes form) for all density ratios at $G < 155$. The present research focused on density ratios of 2.5 and 5.

Brandt and Coletti (2022) recently reviewed homogeneous and wall-bounded turbulent flows laden with inertial spherical particles. Numerous analytical and numerical studies have been conducted to capture the physics associated with particle-fluid-wall interactions. Analytical methods have been discussed for the sedimentation of single spherical (Ferreira and Chhabra, 1998) and non-spherical particles (Yaghoobi and Torabi, 2012). Immersed boundary methods, such as LBM-IBM-HSMD (Habte and Wu, 2017), direct forcing IBM (Eshghinejadfard et al., 2016), boundary thickness-based direct forcing IBM (Qin et al., 2023), IBM-DEM (Derakhshani et al., 2017), and interpolated bounce back LBM-DEM (Pu et al., 2023), have also been employed for single particle studies.

Ghosh (2020) simulated the settling of a permeable circular particle confined between two walls in 2D with immersed boundary methods. Ma et al. (2019) studied the hydrodynamic characteristics of both spheroidal and non-spherical particles in fluid considering particle-particle and particle-wall collisions using the fictitious domain method-discrete element method. Dabic et al. (2016) also used DEM to simulate the deflection of particles in fluid flows due to acoustically induced forces. Prakash et al. (2007) used Smoothed Particle Hydrodynamics (SPH) to simulate the suspension of low-density cylinders (specific gravity = 0.5) in a tank of water mixed by a paddle.

Research investigations most relevant to our work have considered particle sizes ranging from 0.5 mm to 15.94 mm (Xu et al., 2019; Habte and Wu, 2017; Eshghinejadfard et al., 2016; Qin et al., 2023; Tao et al., 2017; Kaur et al., 2019; Chhabra, 1995; Pu et al., 2023; Mohammad and Munshi, 2023), and particle densities ranging from 2,200 kg/m^3 to 7,900 kg/m^3 (Xu et al., 2019; Habte and Wu, 2017; Derakhshani et al., 2017; Kaur et al., 2019; Chhabra, 1995; Mohammad and Munshi, 2023). The channel widths considered in the literature vary from 1.05 to 257 times the particle diameter (Tao et al., 2017; Chhabra, 1996; Madhav and Chhabra, 1995; Pu et al., 2023).

The Lattice Boltzmann method (LBM) accurately captures fluid-solid-wall interactions. One-way coupling accounts for the effect of the fluid on a particle, while two-way coupling accounts for the mutual influence between the fluid and the particle. Particle-wall interaction is implicitly captured through flow modification around the particle due to the proximity of the wall, without the actual collision between the particle and the wall.

In previous studies noted above, the sedimentation of a single spherical particle has been investigated using the LBM. However, several technical gaps remain unaddressed. The terminal settling velocity has only been validated for specific particle diameters and densities, with a fixed channel width. Furthermore, previous research did not consider wall effects in their benchmark cases due to computational limitations. The proximity of walls affects the boundary layer around a settling particle. Walls can alter the flow fields around the particle, generating shear layers and vortices that influence the particle's settling velocity. Specifically, the velocity and vorticity magnitude profiles near the particle and along the walls have not been thoroughly analysed. Another crucial gap is identifying the domain width at which vortices disappear for various particle properties.

The main goal of the present work is to contribute to filling the knowledge gaps noted above by conducting a benchmark study on the settling of single spherical particles, considering their physical properties and the effects of the walls. Also, it is desirable to estimate the wall separation distance at which vortices disappear for various particle properties, such as diameter and density. The accuracy of the point-particle method is compared to the resolved particle method. The LBM results are validated against the experimental data of Gibbs et al. (1971). The OpenLB code (Krause et al., 2021) is employed to study four-way coupling physics (particle-fluid-wall interactions) using both point-particle and resolved particle methods.

The major tasks we address here include computing the terminal settling velocity, analysing the velocity and vorticity profiles, and tracking the particle trajectories for spherical particles of different diameters and densities in water. Initially, one-way coupling simulations analyse the effect of a fluid on a particle. Two-way coupling simulations account for the effects of a fluid on a particle and a particle on a fluid. In two-way coupling, a naive non-local forward coupling method and non-local base back backward coupling method employing Van-Wachem smoothing are selected to transfer the drag forces from a fluid to a particle and a particle to a fluid. The one-way and two-way coupling simulations employed Dapelo's (2019) point particle method based on the approaches developed in Trunk et al. (2018) and Krause et al. (2017).

Further, it is useful to analyse the simulated flow fields around the particle. The flow fields obtained from the point particle method are approximate. To validate the flow profiles, the resolved particle method based on

Krause et al.'s (2017) HLBM is used to compare the flow profiles with those produced by the point particle method. After comparing the flow profiles using both methods, a recommendation regarding the range of G for which the point particle method is accurate can be made. In addition, the wall effects, i.e., channel width effects on the flow fields and particle trajectory, are investigated.

This paper is organised into four additional sections. Section 2 briefly introduces the mathematical modelling and numerical methods employed in OpenLB. Section 3 details the simulation settings in OpenLB. Section 4 presents analysis of the simulation results, examining the influences of particle diameter, particle density, and wall interactions. Section 5 summarises the findings and conclusions drawn from the research.

2 Mathematical modelling and numerical methods

The LBM (Succi, 2001; Sukop and Thorne, 2006; Krüger et al., 2017) is well described by the discrete Boltzmann equation using the Bhatnagar-Gross-Krook (BGK) collision operator:

$$\frac{\partial f_i}{\partial t} + c_i \cdot \nabla f_i = \Omega_i(f) = \omega(f^{eq} - f) = \frac{1}{\tau}(f^{eq} - f) \quad (1)$$

wherein, $f_i(\mathbf{x}, \mathbf{c}, t)$ is the particle distribution function evaluated at a point of phase space (**x**, **c**). In other words, it is the probability of finding a particle at a location with a velocity c_i. Ω is the collision operator, representing the rate of change of the particle distribution function due to binary molecular collisions. The BGK collision operator captures the inter-molecular collisions, conserves mass, momentum, and energy, and satisfies the H-theorem (Guo and Shu, 2013). ω is the collision frequency, and τ is the dimensionless relaxation time. The relationship between kinematic viscosity and dimensionless relaxation time is expressed as

$$\nu = c_s^2\left(\tau - \frac{\Delta t}{2}\right) \quad (2)$$

The local equilibrium distribution function (f^{eq}), also known as Maxwell-Boltzmann distribution function is

$$f^{eq}(\mathbf{x}, \mathbf{c}, t) = \frac{\rho}{\left(2\pi RT\right)^{\frac{3}{2}}} \exp\left(-\frac{(\mathbf{c} - \mathbf{u})}{2RT}\right) \quad (3)$$

where, $R = k_b/m$, is the gas constant with molecular mass m and Boltzmann constant k_b. The Maxwell-Boltzmann distribution in equation (3) can be rewritten using second order orthonormal Hermite polynomials, to correct the discretisation errors arising from the velocity sets:

$$f_i^{eq}(t, r) = \omega_i \rho_f \left[1 + 3h^2 c_i u_f^* - \frac{3}{2}h^2 u_f^* \cdot u_f^* + \frac{9}{2}h^4 (c_i * u_f^*)^2\right] \quad (4)$$

In LBM, time is divided into time steps Δt, space is discretised into Lattice space steps Δx, and three dimensional velocity space is discretised into a finite set of vectors (c_o to c_{q-1}). A Lattice is usually specified in the form of DdQq, wherein d is the dimensionality of the problem and q is the dimension of the discrete velocity space. D2Q9, D3Q19, and D3Q27 are the commonly used Lattice models. The values of the Lattice weights ω_i are dependent on the Lattice models. There are 19 discrete velocities (c_i for $i = 0, 1, 2, 3, 4, 5, 6, 7, 8, .., 18$) for the D3Q19 model used in the present work. The Lattice weights for D3Q19 are $\omega_0 = \frac{1}{3}$, $\omega_{1,2,..,6} = \frac{1}{18}$, and $\omega_{7,8,9,...,18} = \frac{1}{36}$. For more details on the Lattice weights and velocity sets, refer to Krüger et al. (2017).

The macroscopic fluid density is $\rho_f = \sum_i f_i$ and the momentum flux is $\rho_f u_f = \sum_i c_i f_i$. u_f is fluid velocity and u_f^* is the equilibrium fluid velocity. The pressure is $p = \rho c_s^2$ with speed of sound $c_s = c/\sqrt{3}$ and $c = \Delta x/\Delta t$. The Chapman-Enskog expansion procedure can be adopted to derive the Navier-Stokes equation from the Boltzmann equation, in the limit of Mach number, $Ma \ll 1$. The LBM employs a two step procedure: collision, and streaming. In the first step, the particles collide and relax according to the equilibrium distribution function f_i^{eq}. The collision process is a local and nonlinear process.

$$f_i^*(\mathbf{x}, t) = f_i(\mathbf{x}, t) - \frac{\Delta t}{\tau}(f_i(\mathbf{x}, t) - f_i^{eq}(\mathbf{x}, t)) \quad (5)$$

Δx is spatial discretisation and Δt is the discrete time step. After completing the collision step, the streaming process involves fluid mass moving to the next neighbour node on the regular discrete position space during one discrete time step. The streaming process is non-local and linear.

$$f_i(\mathbf{x} + c_i \Delta t, t + \Delta t) = f^*(\mathbf{x}, t) \quad (6)$$

The Homogenised Lattice-Boltzmann model (HLBM) employs a single particle distribution function to represent both the continuous fluid and particulate phases as described in Dapelo et al. (2019). As described in Dapelo et al. (2019), a smoothing distance parameter is used to parameterise a continuous transition from a solid particle to the fluid to improve stability and reduce non-physical pressure and velocity fluctuations near particle surfaces.

For one-way coupling, the effect of a fluid on a particle is only considered, while for two-way coupling, the effects of a fluid on a particle and a particle on a fluid are both considered. Dapelo et al.'s (2019, 2020, 2023) Lagrangian point particle method and Krause et al.'s (2017, 2021) HLBM methods are employed from the OpenLB code and their detailed numerical algorithms are included in their respective papers (Dapelo et al., 2019, 2020, 2023; Krause et al., 2017, 2021).

3 Simulation settings

OpenLB code (Krause et al., 2021) is employed to simulate the sedimentation with the Lagrangian point particle (one-way and two-way coupling) and the homogeneous LBM (HLBM).

3.1 Geometry

An indicator cuboid functor in the OpenLB code creates a vertical rectangular box by specifying its length, width, and height. The width and height of the geometry we employed are typically n times the particle diameter, where n ranges from 1.5 to 120. In the case of HLBM, the outer layers of the box are assigned as wall nodes, while all nodes inside the box are set as fluid nodes. In contrast, for the point particle method, all nodes are fluid nodes with periodic boundary conditions in the lateral directions. The fluid and solid nodes are assigned material numbers 1 and 2, respectively. Figure 1 shows the particle geometry for different particle resolutions (N, defined as the number of Lattice points used to represent the particle diameter) in HLBM. The interface between solid and fluid is represented using a continuously varying porosity domain to avoid issues related to pressure fluctuations. Solid particles have a porosity of zero and fluid nodes have a porosity of one. The particle diameters simulated in this work range from 10 μm to 2,000 μm, while the selected particle densities are 2,500 kg/m^3 and 5,000 kg/m^3. Here we simulate water as the fluid with density 1,000 kg/m^3 and kinematic viscosity 10^{-6} m^2/s.

Figure 1 Spherical particle sedimentation in a rectangular channel using different particle resolutions (see online version for colours)

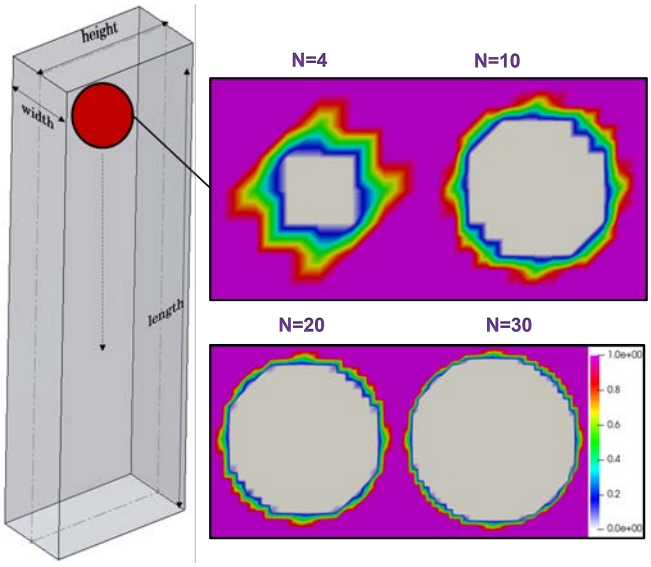

3.2 Initial and boundary conditions

The initial velocities of both the fluid and solid nodes are set to zero. The initial position of the particle is around 20–30% of the total length of the geometry from the top. The particle geometry's resolution is set using the parameter N, where N is the number of Lattice space steps into which the particle diameter is divided. The Lattice density of fluid and solid nodes is set to one. Forced BGK dynamics is employed for one-way and two-way coupling methods. Using OpenLB's HLBM, Porous BGK dynamics, and Smagorinsky Porous BGK dynamics are employed for particle sedimentation in Newtonian fluids.

3.3 Experimental data for validation

The LBM terminal settling velocity simulations are validated against the extensive experimental data of Gibbs et al. (1971). Terminal settling velocity measurements were captured in a 0.128 m diameter tube with a length of 1.24 m. The largest particle diameter considered in the present study is 2,000 μm, while Gibbs et al. (1971) measured the terminal velocity of up to 5,000 μm particles. For the 2,000 μm particle size experimental measurement, the width and height of the rectangular column approximately corresponding to the cylindrical geometry used by Gibbs et al. (1971) would be 64 times the particle diameter. In contrast, for a 10 μm particle, the width and height of the rectangular column approximately corresponding to the experimental cylinder are 12,800 times the particle diameter. In OpenLB and many other numerical approaches, it is computationally challenging to model at resolution adequate to capture the particle-induced flow field over a larger geometric domain because local mesh refinement is not included in the software. Therefore, based on preliminary simulations, the width and height of the rectangular channel are restricted to a maximum of 40 times the particle diameter in our simulations.

4 Results and discussion

In the subsequent sections, the effects of particle diameter and density, and the influence of nearby walls on terminal settling velocity will be assessed. Flow profiles and particle trajectories will be evaluated.

4.1 Comparison between point particle method and HLBM

As noted above, point particle methods can simulate one-way coupling, which accounts for the effect of the fluid on a particle, and two-way coupling, where the effects of a fluid on the particle and a particle on the fluid are both considered. One-way coupling results are valid in the Stokes flow regime.

Figure 2 shows the variation of particle Reynolds number with Galileo number for experimental data and simulations using 2-way point particle and HLBM approaches. The point particle and HLBM methods work well at particle Re less than 1 but are more limited in their ability to accurately simulate particle settling at higher Re. The HLBM approach generally appears to improve the ability to simulate the experimental data at higher Re and G.

Figure 2 Galileo number vs. Reynolds number for experimental data and computed using point particle (two-way coupling method) and HLBM (see online version for colours)

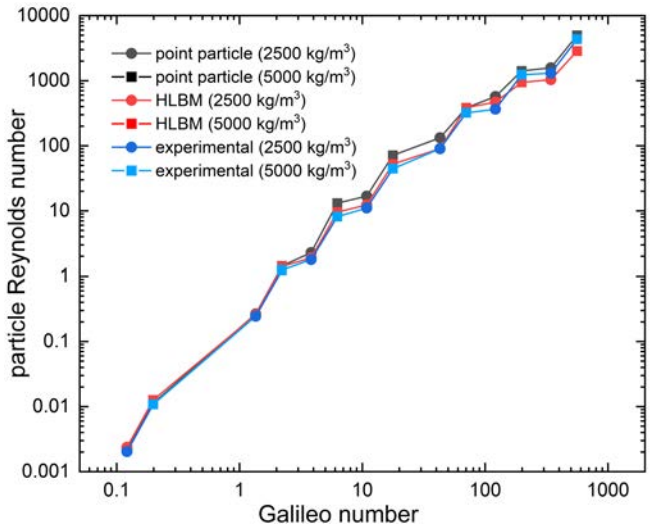

Note: The terminal settling velocity can be computed from the Reynolds number via $u = Re\,\nu/d$.

Figure 3 Velocity magnitude profile for width = height = 40 times particle diameter and particle diameter = 10 μm, (a) point particle and (b) HLBM for particle density = 2,500 kg/m^3 ($\rho_s/\rho = 2.5$, $G = 0.12$) (c) point particle method (d) HLBM for particle density = 5,000 kg/m^3 ($\rho_s/\rho = 5$, $G = 0.2$) (see online version for colours)

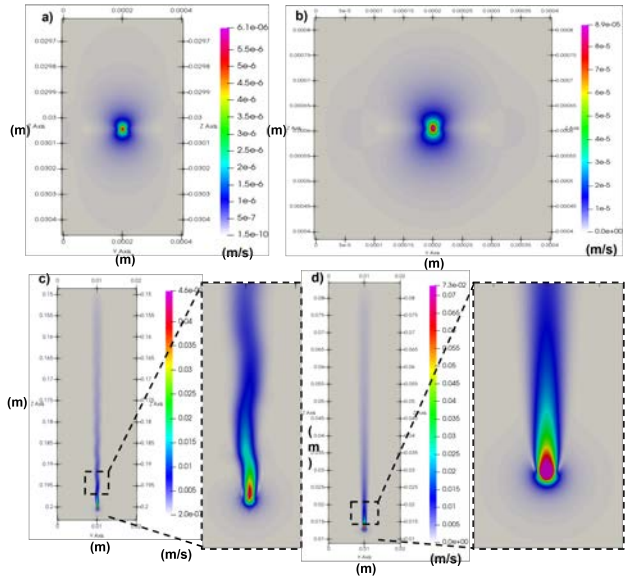

Figure 3 compares the point particle and HLBM approaches for 10 μm particles with 2,500 and 5,000 kg/m^3 densities. The flow profiles are captured more accurately using HLBM because the particle geometry is fully resolved. The point particle method suggests the presence of a sinuous wake behind the particle, while the HLBM approach provides axisymmetric results more consistent with expectations at these low Galileo numbers.

Figure 4 shows the velocity magnitude profiles for a particle density of 2,500 kg/m^3 ($\rho_s/\rho = 2.5$) and particle diameters 10 μm ($G = 0.12$), 50 μm ($G = 1.4$), 100 μm ($G = 3.8$), and 200 μm ($G = 11$). The velocity profiles are axisymmetric. Smaller particle diameters, relatively strong viscous forces, and lower particle inertia leading to low Galileo and Reynolds numbers are responsible for this behaviour. Particle deflection from strictly vertical fall is negligible for smaller particle diameters under the density and viscosity conditions here since the viscous forces dominate over the inertia forces. This maintains symmetry in the velocity flow profile, thereby avoiding lift forces acting on the particle.

Figure 4 Velocity profile using HLBM for particle density = 2,500 kg/m^3 ($\rho_s/\rho = 2.5$), (a) particle diameter = 10 μm (b) particle diameter = 50 μm (c) particle diameter = 100 μm (d) particle diameter = 200 μm (see online version for colours)

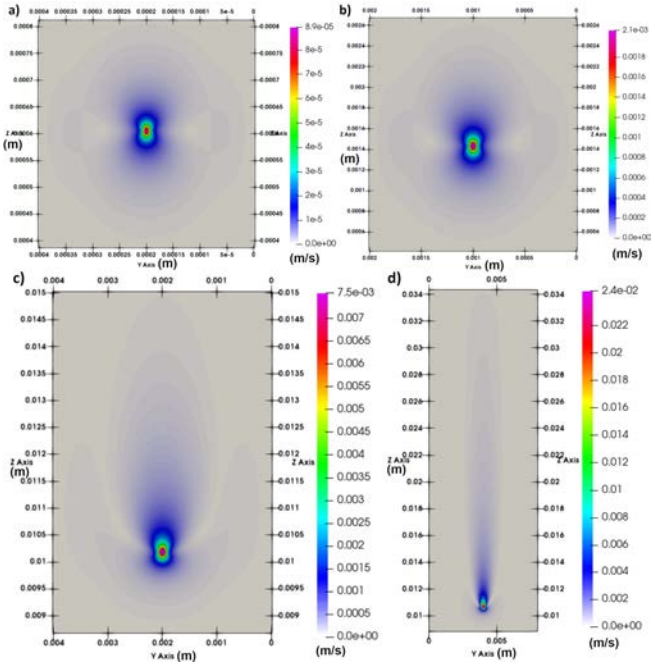

Jenny et al. (2004) showed that the axisymmetric flow patterns break down beyond the Galileo number of 155. Nakamura (1976) found in their experiments that the axisymmetric behaviour breaks down when $Re > 190$. The HLBM simulation results in Figure 5 show that the axisymmetric regime exists for Galileo numbers of at least 43, but breaks down at $G < 120$. Due to higher inertia forces, the 1,000 μm ($G = 120$) and 2,000 μm ($G = 340$) particles are deflected laterally as shown by the particles passing in and out of the plane of the cross-sections of velocity profiles in Figure 5. Hence, the range of conditions leading to axisymmetric flow regimes obtained by HLBM results appears to be narrower ($G < 120$) than the range described in the literature ($G < 155$). This may indicate numerical instability stemming from inadequate resolution as touched on below, but otherwise is not further assessed here.

The dominance of inertial forces is responsible for the development of chaotic flow regimes by settling particles. The chaotic regime is observed for Galileo numbers at and beyond 120 in the HLBM simulations. These results are approximately consistent with Jenny's plot (Jenny et al., 2004) for a variety of settling states as a function of density ratio and Galileo number. Lateral deflection may also move particles closer to the walls, reducing the terminal settling velocity.

Figure 5 Velocity profile using HLBM for particle density = 2,500 kg/m^3 ($\rho_s/\rho = 2.5$), (a) particle diameter = 500 μm (G = 43) (b) particle diameter = 1,000 μm (G = 120) (c) particle diameter = 2,000 μm (G = 340) (see online version for colours)

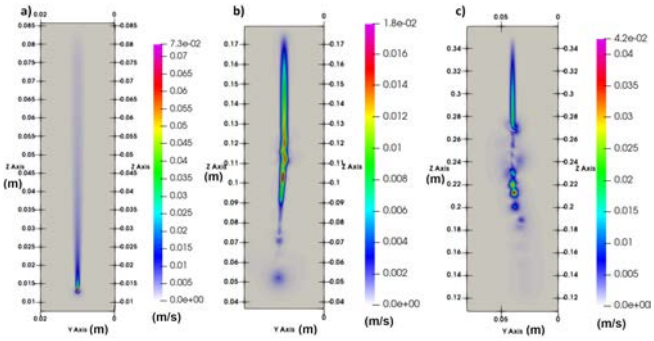

Figure 6 illustrates the vorticity magnitude profiles for particle diameters ranging from 10 μm to 2,000 μm and particle density of 2,500 kg/m^3 ($0.12 < G < 340$). As above, the vorticity magnitude profiles capture the axisymmetric (for $G < 120$) and chaotic flow regimes (for $G > 120$).

Figure 7 compares the vorticity profiles of the numerical results of Rimon and Cheng (1969) with HLBM simulation results.

Rimon and Cheng (1969) used a geometric domain wherein the pipe to sphere diameter ratio is 8.2. In the HLBM results shown in Figure 7, the wall width is 40 times the particle diameter. When the walls are closer to the particle, wake lengths are reduced. In the vorticity profiles of Rimon and Cheng (1969), the wake length is smaller since the walls are closer to the particle. As the particle Reynolds number increases from 10 to 500, the wake length increases correspondingly as shown in Figures 7(c2), 7(c3), 7(c4) and 7(c5). Johnson and Patel (1999) showed similar observations of increased wake length behind a sphere with an increase in Reynolds number.

Figure 8 shows the effects of particle resolution on the particle terminal settling velocity for particle densities of 2,500 kg/m^3 for a range of particle-size-to-wall-separation-width ratios and G from 0.12 to 340. The terminal settling velocities are always smaller when the walls are closer to the particle (e.g., width = height = 1.5, 2.5 times the particle diameter). The terminal settling velocity generally increases with an increase in particle resolution. The shapes of most of these curves suggest that the computed settling velocity has converged (flat) or is converging as N approaches 20.

Figure 6 Vorticity profiles for particle density = 2,500 kg/m^3 ($\rho_s/\rho = 2.5$), width = height = 40 times particle diameter, (a) particle diameter = 10 μm ($G = 0.12$) (b) particle diameter = 50 μm ($G = 1.4$) (c) particle diameter = 100 μm ($G = 6.3$) (d) particle diameter = 200 μm ($G = 11$) (e) particle diameter = 500 μm ($G = 43$) (f) particle diameter = 1,000 μm ($G = 120$) (g) particle diameter = 2,000 μm ($G = 340$) (see online version for colours)

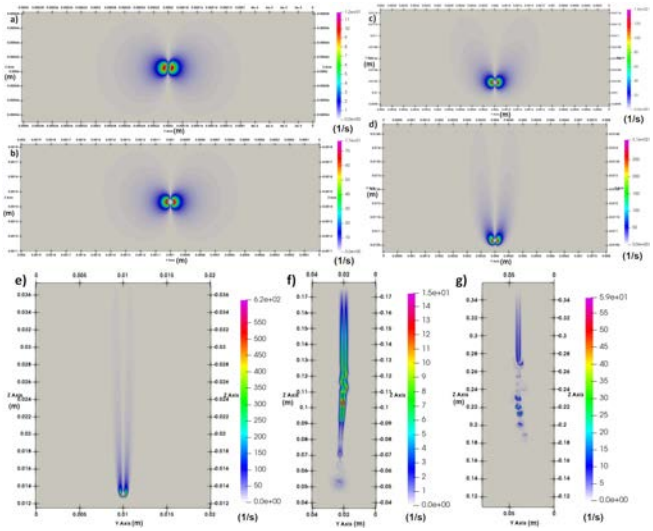

Figure 7 Approximate comparison of numerical results of Rimon and Cheng (1969) with the current LBM results, (a1) Re = 1 (a2) Re_p = 0.002 (b1) Re = 10 (b2) Re_p = 0.09 (c1) Re = 300 (c2) Re_p = 11 (c3) Re_p = 150 (c4) Re_p = 250 (c5) Re_p = 500 (see online version for colours)

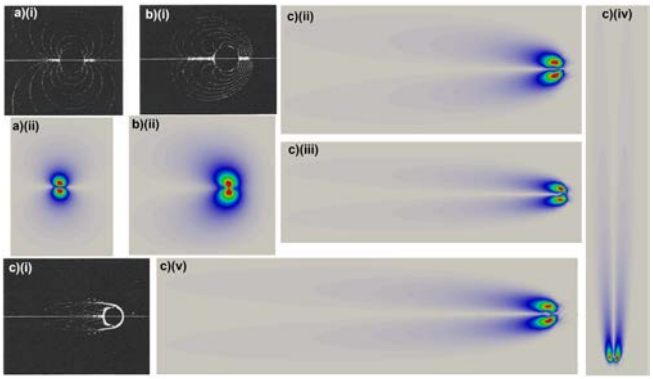

Note: The simulated geometries differ substantially and are reflected in the much longer eddy lengths from the LBM simulations. Permission obtained from AIP publishing to use the figures of numerical results of Rimon and Cheng as shown in Figures 7(a1), 7(b1) and 7(c1).

Figure 8 Resolution effects for particle density = 2,500 kg/m^3 ($\rho_s/\rho = 2.5$) and different wall separation widths (width = height = 1.5, 2.5, 5, 10, 20, 40 times particle diameter as shown on inset legend), (a) particle diameter = 10 μm ($G = 0.12$) (b) particle diameter = 50 μm ($G = 1.4$) (c) particle diameter = 200 μm ($G = 11$) (d) particle diameter = 500 μm ($G = 43$) (e) particle diameter = 1,000 μm ($G = 120$) (f) particle diameter = 2,000 μm ($G = 340$) (see online version for colours)

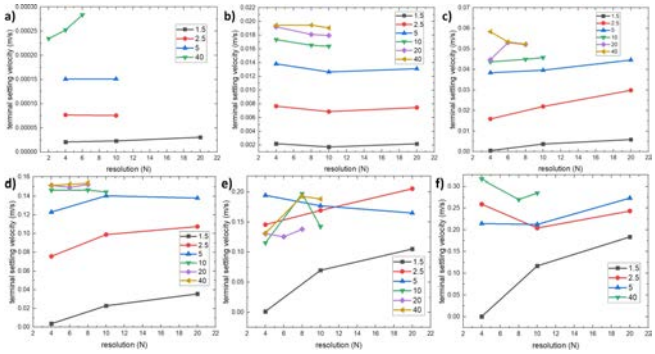

4.2 Wall effects

The terminal settling velocity is typically calculated assuming the flow occurs in an infinite fluid medium. In the present study, the width and height of geometry are n times the particle diameter, where n is a real value. The cases of n primarily considered are $n = 1.5$, 2.5, 5, 10, 20, and 40 times the particle diameter. The reference geometry selected the width and height to be 40 times the particle diameter, wherein the vortices along the walls are small or negligible and the computational burden is not too great.

Figure 9 illustrates the wall effects on the velocity magnitude profiles for a particle diameter of 500 μm and a particle density of 2,500 kg/m^3 ($G = 43$). As the walls get closer to the particle, e.g., width = height = 1.5 times the particle diameter [Figure 9(a)], there is an increase in resistance to the particle's motion and the terminal velocity is significantly reduced. The wake length also decreases. Huang and Feng (1995) also concluded that wall effects contribute to the reduction in wake lengths. As the walls are moved further away [e.g., Figure 9(f)], there is an increase in the wake length and the terminal settling velocity.

Figure 10 demonstrates the percentage reduction in terminal settling velocity from large relative wall separation (12.8 cm diameter tube with maximum particle size 5,000 μm; thus $n > 26$) experimental data from Gibbs et al. (1971) compared to different simulated wall separation widths for a particle density of 2,500 kg/m^3 and particle diameters 10 μm, 200 μm, 1,000 μm and 2,000 μm ($0.12 < G < 340$). The bars are stacked principally in order of relative particle diameter-wall-separation-width n. The first three panels clearly show that the simulations approach the experimental data at n = 20 and, as expected, overshoot the experimental data (for n = 26) when the simulated n is 40.

Figure 9 Velocity magnitude profile for particle diameter = 500 μm, particle density = 2,500 kg/m^3, ($G = 43$), (a) particle resolution (N = 20) and width = height = 1.5 times particle diameter (b) particle resolution (N = 20) and width = height = 2.5 times particle diameter (c) particle resolution (N = 20) and width = height = 5 times particle diameter (d) particle resolution (N = 10) and width = height = 10 times particle diameter (e) particle resolution (N = 8) and width = height = 20 times particle diameter (f) particle resolution (N = 8) and width = height = 40 times particle diameter (see online version for colours)

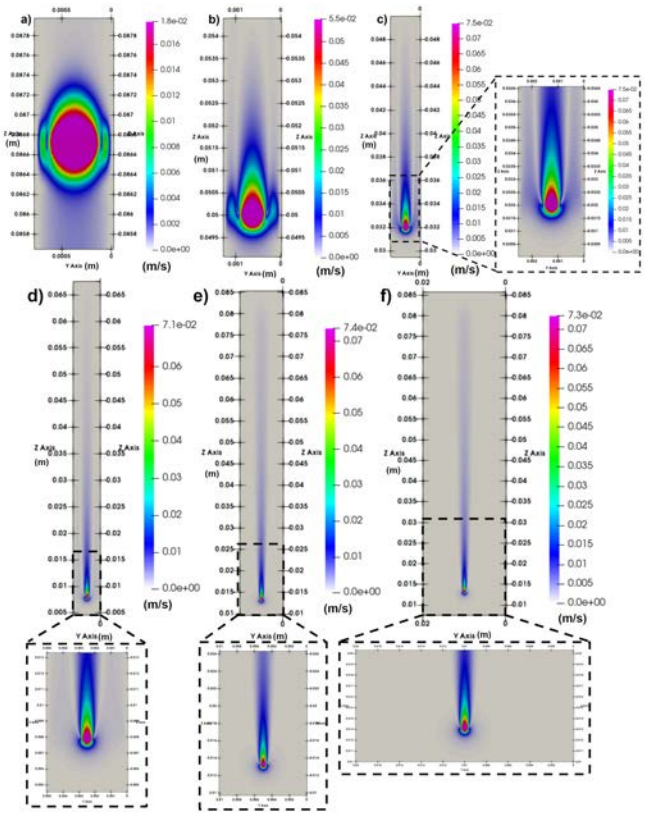

The simulation results for the terminal settling velocity of the largest particle [Figure 10(d); $G = 340$], in contrast, are substantially smaller than the experimental results even at n = 40. As indicated by Figure 8 and shown by the secondary bar stacking according to the resolution (N) in Figure 10, the impact of resolution plays an increasingly important role in the estimates as the particle size exceeds 50 μm (and, more generally, as G exceeds 1.4). Thus, additional resolution of the particle and fluid might well bring the results into better agreement with the experimental data, but the computational cost would be considerably larger.

4.3 Assessment of particle trajectories

The particle trajectories are greatly influenced by particle shape, particle size, particle density, particle rotation, fluid properties, fluid flow regimes, and wall effects.

Figure 10 Percentage reduction in terminal settling velocity w.r.t. experimental data from Gibbs et al. (1971) for particle density = 2,500 kg/m^3, (a) particle diameter = 10 μm (G =0.12) (b) particle diameter = 200 μm (G =11) (c) particle diameter = 1,000 μm (G =120) (d) particle diameter = 2,000 μm (G =340) (see online version for colours)

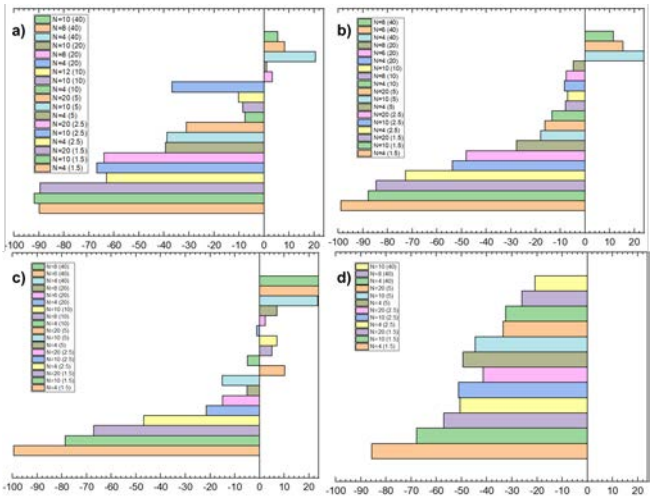

Figure 11 Particle trajectories for particle density = 2,500 kg/m^3 and width = height = 40 times particle diameter, (a) particle diameter = 10 μm (G = 0.12) (b) particle diameter = 200 μm (G = 11) (c) particle diameter = 1,000 μm (G = 120) (d) particle diameter = 2,000 μm (G = 340) (see online version for colours)

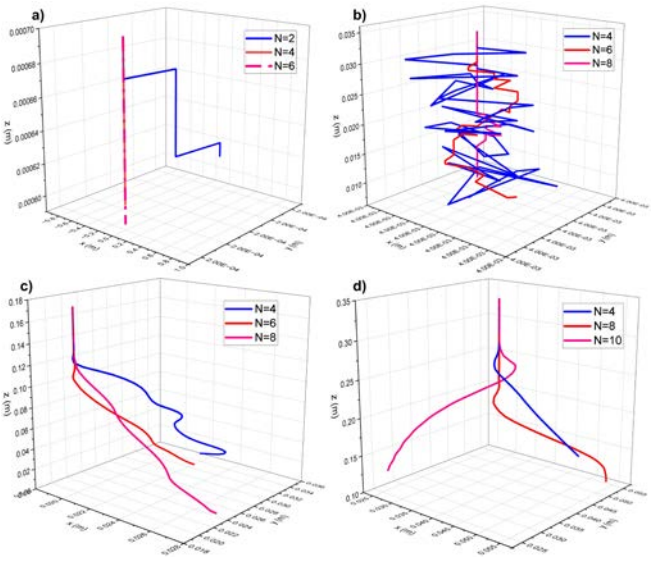

Figure 11 shows the particle trajectory profiles for different particle diameters (10 μm, 200 μm, 1,000 μm, and 2,000 μm) and particle density of 2,500 kg/m^3. For smaller diameter and lighter particles such as 10 μm, 50 μm, 100 μm, and 200 μm (i.e., with $G < 11$, the particle travels in a straight line or laterally depending on the particle resolution. The lateral deflection is in the order of 10^{-4} to 10^{-3} m. As the particle resolution increases from N = 2 to N = 10, the lateral deflections of the particles are also reduced and they follow a straight-line path. A lower resolution particle can have a less-than-perfectly-symmetric geometric representation potentially introducing artefacts into the simulation. At the same time, higher resolution makes simulation of the fluid and particle behaviour more computationally demanding.

There is a velocity gradient perpendicular to the walls of the rectangular channel when particles are moving near the wall. These velocity gradients between the two surfaces induce higher shear stresses in the fluid leading to vortex formation. This leads to the formation of two vortices with unequal vortex intensities on the two sides of the particle surface resulting in lateral deflection of the particle. Veldhuis and Biesheuvel (2007) observed in their experiments that a slightly non-spherical particle can lead to a curved settling path rather than a straight path. These curved paths are also seen in particle trajectories of HLBM results. For higher particle resolutions, the particle geometry may have less apparent asymmetry, the velocity profiles are symmetrical, and no lift forces act on the particle. This prevents erratic motion of the particle.

For larger and denser particles, the lateral deflections are as large as 10^{-2} m (i.e., for $G = 340$). Particle trajectories are erratic and deflect laterally. The fluid flow is in the transition or turbulent flow regime when inertial forces dominate. A transition-turbulent flow regime will increase the hydrodynamic forces acting on the particle. Hence, the torque acting on the particle also increases, increasing the particle's angular velocity. Further, due to the Magnus effect (Magnus, 1853), particles get deflected laterally leading to chaotic particle trajectories.

This erratic particle motion can also be explained by preferential sweeping and particle loitering phenomena. In the preferential sweeping phenomena, the particle motion is pushed in the direction of the low vorticity region. Maxey (1987) observed that inertial particles are centrifuged out of high vorticity regions and accumulate in low vorticity regions. This preferential sweeping mechanism is also seen in experimental (Good et al., 2014; Aliseda et al., 2002) and direct numerical simulation (DNS) studies (Ireland et al., 2016; Monchaux and Dejoan, 2017; Tom et al., 2022). Along with the impacts of particle preferential sweeping, the terminal settling velocity is also reduced due to the loitering phenomenon. Nielsen (1993) first observed the loitering phenomenon. It was also seen in DNS studies (Wang and Maxey, 1993) and experiments (Yang and Shy, 2003; Kawanisi and Shiozaki, 2008).

The particle trajectories of larger diameter and heavier particles (higher G) can be classified as straight, sideways, stepped, and helical. Smaller diameter particles such as 10 μm, 50 μm and 100 μm ($G =< 3.8$) while larger diameter particles (200 μm, 500 μm, 1,000 μm, and 2,000 μm, $G > 11$) have larger inertia and tend to sediment either in a straight line, laterally, or in a helical manner. The lateral movement of larger and heavier particles is restricted and reduced if the walls are close to the particles.

5 Conclusions

The LBM is utilised to investigate the phenomenon of particle settling. Particle settling involves interaction between fluids, particles, and walls. The following are the findings from this research study:

1 The point particle method takes into consideration the effect of the particle on the fluid and the fluid on the particle. The flow profiles computed using it are accurate in the Stokes law regime. The settling velocities are overestimated for particle Reynolds numbers in the transition-turbulent flow regimes.

2 HLBM resolves the flow around the particle. The axisymmetric flow regime is observed for smaller and lighter (lower G) particles, while the chaotic flow regime is captured for larger and heavier (higher G) particles .

3 Wall effects are significant when the walls are closer to the particles. For instance, when the width = height = 1.5 times the particle diameter, the percentage reduction in terminal settling is highest for smaller diameter and lighter particles (lower G). As the particle becomes larger and heavier (higher G), the reduction in terminal settling velocity keeps decreasing. Further, the wake lengths reduce drastically for the larger diameter and heavier particles compared to the smaller diameter and lighter particles. Wall effects become small or negligible when the wall width is 40 times the particle diameter. The disappearance of vortices along the wall indicates the absence of wall effects.

4 Particle shape, particle diameter, particle density, and closeness of walls influence the trajectory of the particle. The lateral movement of small diameter particles (lower G) is of the order of 10^{-4} m to 10^{-3} m, since the viscous forces are dominant. For larger diameter particles (higher G), the lateral movement is of the order of 10^{-2} m. Inertial forces, particle asymmetry, and the Magnus effect contribute to the lateral movement of these particles.

To conclude, improved knowledge of the physics of particle-fluid and particle-wall interactions captured from single-particle Lattice Boltzmann simulations can serve as a building block towards understanding the settling behaviour of multiple particles and aiding operators in industries to make informed decisions.

Funding

This project was funded by the Department of Energy (DoE), Minority Serving Institution Partnership Program (MSIPP), under Task Order No. 0000663597.

Declarations

All authors declare that they have no conflicts of interest.

References

Aliseda, A., Cartellier, A., Hainaux, F., and Lasheras, J.C. (2002) 'Effect of preferential concentration on the settling velocity of heavy particles in homogeneous isotropic turbulence', *Journal of Fluid Mechanics*, Vol. 468, pp.77–105, DOI: 10.1017/S0022112002001593.

Brandt, L. and Coletti, F. (2022) 'Particle-laden turbulence: progress and perspectives', *Annual Review of Fluid Mechanics*, Vol. 54, No. 1, pp.159–189, DOI: 10.1146/annurev-fluid-030121-021103.

Chhabra, R. (1995) 'Wall effects on free-settling velocity of non-spherical particles in viscous media in cylindrical tubes', *Powder Technology*, Vol. 85, No. 1, pp.83–90, DOI: 10.1016/0032-5910(95)03012-X.

Chhabra, R. (1996) 'Wall effects on terminal velocity of non-spherical particles in non-Newtonian polymer solutions', *Powder Technology*, Vol. 88, No. 1, pp.39–44, DOI: 10.1016/0032-5910(96)03100-2.

Dabic, M., Deglon, D.A. and Meyer, C.J. (2016) 'CFD-DEM simulation of fluid suspended particle response behaviour subject to transverse acoustic standing fields', *Progress in Computational Fluid Dynamics, An International Journal*, Vol. 16, No. 1, p.1, https://doi.org/10.1504/PCFD.2016.074223.

Dapelo, D., Kummerländer, A., Krause, M.J. and Bridgeman, J. (2023) 'Lattice-Boltzmann les modelling of a full-scale, biogas-mixed anaerobic digester', *Engineering with Computers*, Vol. 40, pp.1–25.

Dapelo, D., Trunk, R., Krause, M.J. and Bridgeman, J. (2019) 'Towards Lattice-Boltzmann modelling of unconfined gas mixing in anaerobic digestion', *Computers & Fluids*, Vol. 180, pp.11–21, DOI: 10.1016/j.compfluid.2018.12.008.

Dapelo, D., Trunk, R., Krause, M.J., Cassidy, N., and Bridgeman, J. (2020) 'The application of Buckingham π theorem to Lattice-Boltzmann modelling of sewage sludge digestion', *Computers & Fluids*, Vol. 209, Article No. 104632.

Derakhshani, S.M., Schott, D.L., and Lodewijks, G. (2017) 'Modeling particle sedimentation in viscous fluids with a coupled immersed boundary method and discrete element method', *Particuology*, Vol. 31, pp.191–199, DOI: 10.1016/j.partic.2016.09.006.

Eshghinejadfard, A., Abdelsamie, A., Janiga, G. and Thévenin, D. (2016) 'Direct-forcing immersed boundary Lattice Boltzmann simulation of particle/fluid interactions for spherical and non-spherical particles', *Particuology*, Vol. 25, pp.93–103, DOI: 10.1016/j.partic.2015.05.004.

Ferreira, J. and Chhabra, R. (1998) 'Accelerating motion of a vertically falling sphere in incompressible Newtonian media: an analytical solution', *Powder Technology*, Vol. 97, No. 1, pp.6–15, DOI: 10.1016/S0032-5910(97)03386-X.

Ghosh, S. (2020) 'Immersed boundary method for a permeable sedimenting circular particle between two parallel rigid walls', *Progress in Computational Fluid Dynamics, An International Journal*, Vol. 20, No. 1, p.20, https://doi.org/10.1504/PCFD.2020.104708.

Gibbs, R.J., Matthews, M.D. and Link, D.A. (1971) 'The relationship between sphere size and settling velocity', *Journal of Sedimentary Research*, Vol. 41, No. 1, pp.7–18, DOI: 10.1306/74D721D0-2B21-11D7- 8648000102C1865D.

Good, G., Ireland, P., Bewley, G., Bodenschatz, E., Collins, L. and Warhaft, Z. (2014) 'Settling regimes of inertial particles in isotropic turbulence', *Journal of Fluid Mechanics*, Vol. 759, p.R3, DOI: 10.1017/jfm.2014.602.

Guo, Z. and Shu, C. (2013) *Lattice Boltzmann Method and Its Application in Engineering*, Vol. 3, World Scientific, Singapore.

Habte, M.A. and Wu, C. (2017) 'Particle sedimentation using hybrid Lattice Boltzmann-immersed boundary method scheme', *Powder Technology*, Vol. 315, pp.486–498, DOI: 10.1016/j.powtec.2017.04.032.

Huang, P. and Feng, J. (1995) 'Wall effects on the flow of viscoelastic fluids around a circular cylinder', *Journal of Non-Newtonian Fluid Mechanics*, Vol. 60, Nos. 2–3, pp.179–198, DOI: 10.1016/0377-0257(95)01394-2..

Ireland, P.J., Bragg, A.D. and Collins, L.R. (2016) 'The effect of Reynolds number on inertial particle dynamics in isotropic turbulence. Part 2. Simulations with gravitational effects', *Journal of Fluid Mechanics*, Vol. 796, pp.659–711, DOI: 10.1017/jfm.2016.227.

Jenny, M., Dušek, J. and Bouchet, G. (2004) 'Instabilities and transition of a sphere falling or ascending freely in a Newtonian fluid', *Journal of Fluid Mechanics*, Vol. 508, pp.201–239, DOI: 10.1017/S0022112004009164.

Johnson, T. and Patel, V. (1999) 'Flow past a sphere up to a Reynolds number of 300', *Journal of Fluid Mechanics*, Vol. 378, pp.19–70, DOI: 10.1017/S0022112098003206.

Kaur, A., Sobti, A., Toor, A.P. and Wanchoo, R.K. (2019) 'Motion of spheres and cylinders in viscoelastic fluids: asymptotic behavior', *Powder Technology*, Vol. 345, pp.82–90, DOI: 10.1016/j.powtec.2018.12.073.

Kawanisi, K. and Shiozaki, R. (2008) 'Turbulent effects on the settling velocity of suspended sediment', *Journal of Hydraulic Engineering*, Vol. 134, No. 2, pp.261–266, DOI: 10.1061/(ASCE)0733-9429(2008)134:2(26.

Krause, M.J., Klemens, F., Henn, T., Trunk, R. and Nirschl, H. (2017) 'Particle flow simulations with homogenised Lattice Boltzmann methods', *Particuology*, Vol. 34, pp.1–13, DOI: 10.1016/j.partic.2016.11.001.

Krause, M.J., Kummerländer, A., Avis, S.J., Kusumaatmaja, H., Dapelo, D., Klemens, F., Gaedtke, M., Hafen, N., Mink, A., Trunk, R. et al. (2021) 'OpenLB-Open source Lattice Boltzmann code', *Computers & Mathematics with Applications*, Vol. 81, pp.258–288, DOI: 10.1016/j.camwa.2020.04.033.

Krüger, T., Kusumaatmaja, H., Kuzmin, A., Shardt, O., Silva, G. and Viggen, E.M. (2017) *The Lattice Boltzmann Method*, Springer International Publishing, Vol. 10, No. 978-3, pp.4–15, DOI: 10.1007/978-3-319-44649-3.

Ma, S., Wei, Z., Chen, X. and Lin, Q. (2019) 'Fictitious domain method combined with the DEM for studying particle-particle/particle-wall collision in fluid', *Progress in Computational Fluid Dynamics, An International Journal*, Vol. 19, No. 2, p.80, https://doi.org/10.1504/PCFD.2019.098481.

Madhav, G.V. and Chhabra, R. (1995) 'Drag on non-spherical particles in viscous fluids', *International Journal of Mineral Processing*, Vol. 43, Nos. 1–2, pp.15–29, DOI: 10.1016/0301-7516(94)00038-2.

Magnus, H.G. (1853) *Über die Abweichung der Geschosse*, Druckerei der Königlichen Akademie der Wissenschaften, Berlin.

Maxey, M.R. (1987) 'The gravitational settling of aerosol particles in homogeneous turbulence and random flow fields', *Journal of Fluid Mechanics*, Vol. 174, pp.441–465, DOI: 10.1017/S0022112087000193.

Mohammad, H. and Munshi, B. (2023) 'Experimental study of wall effect on hollow cylindrical particle settling in Newtonian and non-Newtonian fluids in cylindrical channels', *Powder Technology*, Vol. 428, p.118858, DOI: 10.1016/j.powtec.2023.118858.

Monchaux, R. and Dejoan, A. (2017) 'Settling velocity and preferential concentration of heavy particles under two-way coupling effects in homogeneous turbulence', *Physical Review Fluids*, Vol. 2, No. 10, p.104302, DOI: 10.1103/PhysRevFluids.2.104302.

Nakamura, I. (1976) 'Steady wake behind a sphere', *The Physics of Fluids*, Vol. 19, No. 1, pp.5–8, DOI: 10.1063/1.861328.

Nielsen, P. (1993) 'Turbulence effects on the settling of suspended particles', *Journal of Sedimentary Research*, Vol. 63, No. 5, pp.835–838, DOI: 10.1306/D4267C1C-2B26-11D7-8648000102C1865D.

Prakash, M., Cleary, P.W., Ha, J., Mehidi, M.N.N., Blackburn, H.M. and Brooks, G. (2007) 'Simulation of suspension of solids in a liquid in a mixing tank using SPH and comparison with physical modelling experiments', *Progress in Computational Fluid Dynamics, An International Journal*, Vol. 7, Nos. 2/3/4, p.91, https://doi.org/10.1504/PCFD.2007.013001.

Pu, D., Li, M., Shen, L., Wang, Z. and Li, Z. (2023) 'The effects of channel width on particle sedimentation in fluids using a coupled Lattice Boltzmann-discrete element model', *Physics of Fluids*, Vol. 35, No. 5, DOI: 10.1063/5.0147826.

Qin, S., Jiang, M., Ma, K., Su, J. and Liu, Z. (2023) 'Fully resolved simulations of viscoelastic suspensions by an efficient immersed boundary-Lattice Boltzmann method', *Particuology*, Vol. 75, pp.26–49, DOI: 10.1016/j.partic.2022.06.004.

Rimon, Y. and Cheng, S. (1969) 'Numerical solution of a uniform flow over a sphere at intermediate Reynolds numbers', *The Physics of Fluids*, Vol. 12, No. 5, pp.949–959, DOI: 10.1063/1.2163685.

Succi, S. (2001) *The Lattice Boltzmann Equation: For Fluid Dynamics and Beyond*, Oxford University Press, Oxford, DOI: 10.1093/oso/9780198503989.001.0001.".

Sukop, M.C. and Thorne Jr., D.T. (2006) *Lattice Boltzmann Modeling: An Introduction for Geoscientists and Engineers*, Springer, Berlin, DOI: 10.1007/978-3-540-27982-2.

Tao, S., Guo, Z. and Wang, L-P. (2017) 'Numerical study on the sedimentation of single and multiple slippery particles in a Newtonian fluid', *Powder Technology*, Vol. 315, pp.126–138, DOI: 10.1016/j.powtec.2017.03.039.

Tom, J., Carbone, M. and Bragg, A.D. (2022) 'How does two-way coupling modify particle settling and the role of multiscale preferential sweeping?', *Journal of Fluid Mechanics*, Vol. 947, p.A7, DOI: 10.1017/jfm.2022.615.

Trunk, R., Marquardt, J., Thäter, G., Nirschl, H. and Krause, M.J. (2018) 'Towards the simulation of arbitrarily shaped 3D particles using a homogenised Lattice Boltzmann method', *Computers & Fluids*, Vol. 172, pp.621–631, https://doi.org/10.1016/j.compfluid.2018.02.027.

Veldhuis, C. and Biesheuvel, A. (2007) 'An experimental study of the regimes of motion of spheres falling or ascending freely in a Newtonian fluid', *International Journal of Multiphase Flow*, Vol. 33, No. 10, pp.1074–1087, DOI: 10.1016/j.ijmultiphaseflow.2007.05.002.

Wang, L-P. and Maxey, M.R. (1993). Settling velocity and concentration distribution of heavy particles in homogeneous isotropic turbulence', *Journal of Fluid Mechanics*, Vol. 256, pp.27–68, DOI: 10.1017/S0022112093002708.

Wray, E. (1977) 'Stokes' law revisited', *Physics Education*, Vol. 12, No. 5, p.300, DOI: 10.1088/0031-9120/12/5/006.

Xu, Z., Song, X., Li, G., Pang, Z. and Zhu, Z. (2019) 'Settling behavior of non-spherical particles in power-law fluids: experimental study and model development', *Particuology*, Vol. 46, pp.30–39, DOI: 10.1016/j.partic.2018.07.006.

Yaghoobi, H. and Torabi, M. (2012) 'Analytical solution for settling of non-spherical particles in incompressible Newtonian media', *Powder Technology*, Vol. 221, pp.453–463, DOI: 10.1016/j.powtec.2012.01.044.

Yang, T. and Shy, S. (2003) 'The settling velocity of heavy particles in an aqueous near-isotropic turbulence', *Physics of Fluids*, Vol. 15, No. 4, pp.868–880, DOI: 10.1063/1.1557526.